CHAPTER 4

THREE-NODE SHELL ELEMENT (REISSNER–MINDLIN PLATE THEORY)

Many developments discussed in Chapter 3 are dealt with warping of curved surface for the four-node quadrilateral elements. This concern has led us to revisit the triangular element. The three-node triangular element with linear interpolation is always flat and has no warping. On the other hand, as discussed in Section 3.8.2, the locking-free element with rectangular mesh could lose convergence rate when extended to general quadrilateral mesh due to the nonconstant Jacobian. The three-node triangular element always has constant Jacobian. There is no need of a special mesh once an element is proven to be locking-free. Triangular mesh is also more flexible in modeling complex geometry.

The triangular element has been in demand as a candidate for solving the bending problems. It has been, however, another long journey to find a better answer. Obviously, with low order interpolation, shear locking is still a problem with the three-node triangular element based on R-M theory. The four-node quadrilateral element has a natural structure with tensor product, which, unfortunately does not exist in the triangular element. Some techniques developed for quadrilateral elements are not directly applicable to the triangular elements. It is found that in many applications, people prefer quadrilateral mesh to the triangular mesh due to the concern about the stiff C^0 element. Some researchers have even warned against the use of triangular mesh except in areas where the geometry is difficult to be meshed by quads. This exception is still conditional, for example, with limit on the total number of triangles to be less than a few percentages of the whole model.

Introduction to the Explicit Finite Element Method for Nonlinear Transient Dynamics, First Edition.
Shen R. Wu and Lei Gu.
 Published 2012 by John Wiley & Sons, Inc.

In this chapter, we discuss some of the developments in triangular elements, including the projection method and the discrete Kirchhoff theory.

4.1 FUNDAMENTALS OF A THREE-NODE C^0 ELEMENT

4.1.1 Transformation and Jacobian

The isoparametric element is considered for the three-node triangles. The linear interpolation uses the following shape functions:

$$\begin{aligned} \varphi_1 &= 1 - \xi - \eta, \\ \varphi_2 &= \xi, \\ \varphi_3 &= \eta. \end{aligned} \tag{4.1}$$

A general triangle in O-XY plane is mapped to the master isosceles right-angled triangle depicted in Figure 4.1 by

$$\begin{aligned} x &= \sum x_J \varphi_J(\xi, \eta), \\ y &= \sum y_J \varphi_J(\xi, \eta). \end{aligned} \tag{4.2}$$

The Jacobian is

$$\begin{aligned} \boldsymbol{J} &= \frac{\partial(x, y)}{\partial(\xi, \eta)} = \begin{bmatrix} x_\xi & x_\eta \\ y_\xi & y_\eta \end{bmatrix} = \begin{bmatrix} x_2 - x_1 & x_3 - x_1 \\ y_2 - y_1 & y_3 - y_1 \end{bmatrix}, \\ D &= \det(\boldsymbol{J}) = (x_2 - x_1)(y_3 - y_1) - (x_3 - x_1)(y_2 - y_1) = 2A. \end{aligned} \tag{4.3}$$

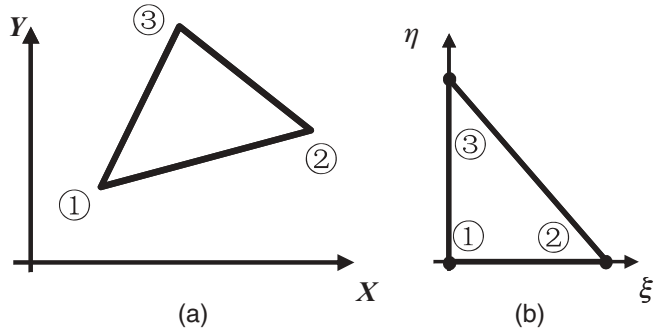

FIGURE 4.1 Three-node triangular element: (a) in the physical domain; (b) in the reference plane.

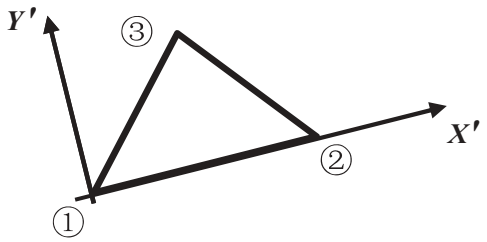

FIGURE 4.2 Local system of the triangular element.

Here, A is the area of the triangle. The inverse of Jacobian is

$$\boldsymbol{J}^{-1} = \frac{\partial(\xi, \eta)}{\partial(x, y)} = \begin{bmatrix} \xi_x & \xi_y \\ \eta_x & \eta_y \end{bmatrix} = \frac{1}{D}\begin{bmatrix} y_\eta & -x_\eta \\ -y_\xi & x_\xi \end{bmatrix}$$

$$= \frac{1}{D}\begin{bmatrix} y_3 - y_1 & x_1 - x_3 \\ y_1 - y_2 & x_2 - x_1 \end{bmatrix}. \tag{4.4}$$

All the transformations are linear with constant Jacobians.

We consider a simple way to define the local system proposed by Belytschko et al. (1984), depicted in Figure 4.2. In this situation, we have $x_1 = y_1 = y_2 = 0$. The Jacobian and its inverse are simplified as

$$\overline{\boldsymbol{J}} = \begin{bmatrix} x_2 & x_3 \\ 0 & y_3 \end{bmatrix},$$

$$D = x_2 y_3, \tag{4.5}$$

$$\overline{\boldsymbol{J}}^{-1} = \frac{1}{x_2 y_3}\begin{bmatrix} y_3 & -x_3 \\ 0 & x_2 \end{bmatrix}.$$

The derivatives of the shape functions are

$$\begin{bmatrix} \dfrac{\partial \varphi_J}{\partial x} \end{bmatrix} = \begin{bmatrix} \dfrac{\partial \varphi_J}{\partial \xi}\xi_x + \dfrac{\partial \varphi_J}{\partial \eta}\eta_x \end{bmatrix} = \frac{1}{x_2 y_3}\begin{bmatrix} -y_3 \\ y_3 \\ 0 \end{bmatrix},$$

$$\begin{bmatrix} \dfrac{\partial \varphi_J}{\partial y} \end{bmatrix} = \begin{bmatrix} \dfrac{\partial \varphi_J}{\partial \xi}\xi_y + \dfrac{\partial \varphi_J}{\partial \eta}\eta_y \end{bmatrix} = \frac{1}{x_2 y_3}\begin{bmatrix} x_3 - x_2 \\ -x_3 \\ x_2 \end{bmatrix}. \tag{4.6}$$

4.1.2 Numerical Quadrature for In-plane Integration

Consider integration over the master element. We have the following for the monomials:

$$\begin{aligned}
&\iint 1 \mathrm{d}\xi \mathrm{d}\eta = 1/2, \\
&\iint \xi \mathrm{d}\xi \mathrm{d}\eta = \iint \eta \mathrm{d}\xi \mathrm{d}\eta = 1/6, \\
&\iint \xi^2 \mathrm{d}\xi \mathrm{d}\eta = \iint \eta^2 \mathrm{d}\xi \mathrm{d}\eta = 1/12, \\
&\iint \xi\eta \mathrm{d}\xi \mathrm{d}\eta = 1/24.
\end{aligned} \tag{4.7}$$

When devicing a numerical integration, we use

$$\iint f(\xi, \eta) \mathrm{d}\xi \mathrm{d}\eta \approx \sum w_j f(\xi_j, \eta_j). \tag{4.8}$$

We notice the difference from that of the quadrilateral element. The latter utilizes the structure of tensor product, which does not exist in the triangular element. The traditional Gauss quadrature used for quadrilateral element does not apply to the triangular element. Therefore, we need a different rule: a tri-symmetric method. That means if we use one-point quadrature, the integration point should be the centroid, which has coordinates $(1/3, 1/3)$ in the master element. In higher order, a set of three points with identical weights is a basic structure for the integration rule.

We can verify:

1. Quadrature with one point at element center $(1/3, 1/3)$ and weight $w = 1/2$ can make exact integration up to linear terms;
2. Quadrature with three points at mid-side points $(1/2, 0)$, $(1/2, 1/2)$, and $(0, 1/2)$, and weight $w_j = 1/6$ can make exact integration up to quadratic terms.

4.1.3 Shear Locking with C^0 Triangular Element

Similar to the situation discussed in Chapter 3, the three-node triangular bending element based on R-M theory has a shear locking issue.

For simplicity, consider an example with the master element. Assume a pure bending mode with nodal deflection and rotations as

$$\begin{aligned}
&w_J = \beta_{yJ} = 0, \quad J = 1, 2, 3, \\
&\beta_{x1} = \beta_{x3} = -\alpha, \quad \beta_{x2} = \alpha.
\end{aligned} \tag{4.9}$$

Using interpolation with the shape functions (4.1), we have

$$\begin{aligned}
w &\equiv 0, \\
\beta_x &= -\alpha(1 - x - y) + \alpha x - \alpha y = \alpha(-1 + 2x), \\
\gamma^h_{xz} &= w_{,x} - \beta_x = \alpha(1 - 2x) \neq 0.
\end{aligned} \tag{4.10}$$

The linear interpolation results in a nonzero transverse shear strain. As discussed in Chapter 3, the bending stiffness is proportional to ζ^3 (ζ is the thickness) while the shear stiffness is proportional to ζ. When the thickness becomes small, the nonzero transverse shear strain energy will dominate the bending strain energy. This results in shear locking.

One-point reduced integration has been used for the quadrilateral shell element to avoid shear locking, in the unique situation that the shear strain is zero at the integration point. For the C^0 triangular element, three-point quadrature is needed to fully integrate the shear strain energy for elasticity. From (4.1), however, we realize that the one-point reduced quadrature at (1/3, 1/3) does not eliminate the shear strain.

In the history of explicit software development, efficient C^0 quadrilateral element, such as B-T element with good accuracy, has been available earlier than the counterpart of C^0 triangular element. The C^0 triangular element used to be considered too stiff and therefore was recommended to be avoided or to be applied sparingly.

4.2 DECOMPOSITION METHOD FOR C^0 TRIANGULAR ELEMENT WITH ONE-POINT INTEGRATION

4.2.1 A C^0 Element with Decomposition of Deflection

Among many efforts towards obtaining a reliable and efficient C^0 triangular element, Belytschko et al. (1984) proposed a decomposition method for the plate bending element. The deflection and rotations of the normal were decomposed to study the contributions to bending energy and shear energy. We describe the fundamentals in this section. Symbolically, let

$$\begin{aligned} w &= w^b + w^s, \\ \beta_\alpha &= \beta_\alpha^b + \beta_\alpha^s. \end{aligned} \tag{4.11}$$

Correspondingly, the strain and the curvature are decomposed into two parts, which are indicated by superscripts b and s for bending and transverse shear, respectively,

$$\begin{aligned} \gamma_\alpha &= \gamma_\alpha^b + \gamma_\alpha^s = w_{,\alpha} - \beta_\alpha, \\ \kappa_{\alpha\beta} &= \kappa_{\alpha\beta}^b + \kappa_{\alpha\beta}^s = -(\beta_{\alpha,\beta} + \beta_{\beta,\alpha}). \end{aligned} \tag{4.12}$$

Note that the quoted paper used different definition for normal rotations. Here, β_x and β_y correspond to $-\theta_x$ and $-\theta_y$ in the reference paper.

For simplicity, we consider the local system shown in Figure 4.2 and the Jacobian of (4.5). Then, (4.12) is rewritten in vector form as

$$
\begin{aligned}
(\boldsymbol{\beta}, w)^T &= (\beta_{1x}, \beta_{1y}, \beta_{2x}, \beta_{2y}, \beta_{3x}, \beta_{3y}, w_1, w_2, w_3), \\
\boldsymbol{\kappa} &= \boldsymbol{B}^b \begin{bmatrix} \boldsymbol{\beta} \\ w \end{bmatrix}, \quad \boldsymbol{\gamma} = \boldsymbol{B}^s \begin{bmatrix} \boldsymbol{\beta} \\ w \end{bmatrix}, \\
(\boldsymbol{B^b})_{3\times 9} &= \left(\boldsymbol{B}_r^b, \boldsymbol{O}_{3\times 3}\right), \quad (\boldsymbol{B}^s)_{2\times 9} = \left(\boldsymbol{B}_r^s, \boldsymbol{B}_d^s\right).
\end{aligned} \tag{4.13}
$$

Here, the differential operators are also decomposed. The subscripts r and d are for the contributions from rotations and deflection respectively. Using (4.6), we have

$$
\begin{aligned}
\left(\boldsymbol{B}_r^b\right)_{3\times 6} &= \frac{-1}{x_2 y_3} \begin{bmatrix} -y_3 & 0 & y_3 & 0 & 0 & 0 \\ 0 & x_3 - x_2 & 0 & -x_3 & 0 & x_2 \\ x_3 - x_2 & -y_3 & -x_3 & y_3 & x_2 & 0 \end{bmatrix}, \\
\left(\boldsymbol{B}_r^s\right)_{2\times 6} &= -\begin{bmatrix} \varphi_1 & 0 & \varphi_2 & 0 & \varphi_3 & 0 \\ 0 & \varphi_1 & 0 & \varphi_2 & 0 & \varphi_3 \end{bmatrix}, \\
\left(\boldsymbol{B}_d^s\right)_{2\times 3} &= \frac{1}{x_2 y_3} \begin{bmatrix} -y_3 & y_3 & 0 \\ x_3 - x_2 & -x_3 & x_2 \end{bmatrix}.
\end{aligned} \tag{4.14}
$$

In many applications, bending is the main deformation mode and the bending strain energy is the main part of deformation energy. With the concept of decomposition, we assume that only the bending mode contributes to the bending energy and only the shear mode contributes to the shear strain energy. For linear elasticity, the strain energy is decomposed:

$$
\begin{aligned}
2U &= \int_A \left((\kappa^b)^T D_b \kappa^b + (\gamma^s)^T D_s \gamma^s\right) \mathrm{d}A \\
&= \int_A \left((\boldsymbol{\beta}^b, w^b)(\boldsymbol{B}^b)^T \boldsymbol{D}_b \boldsymbol{B}^b \begin{bmatrix} \boldsymbol{\beta}^b \\ w^b \end{bmatrix} + (\boldsymbol{\beta}^s, w^s)(\boldsymbol{B}^s)^T \boldsymbol{D}_s \boldsymbol{B}^s \begin{bmatrix} \boldsymbol{\beta}^s \\ w^s \end{bmatrix} \right) \mathrm{d}A,
\end{aligned} \tag{4.15a}
$$

$$
\begin{aligned}
\boldsymbol{D}_b &= \frac{E\zeta^3}{12(1-\nu^2)} \begin{bmatrix} 1 & \nu & 0 \\ \nu & 1 & 0 \\ 0 & 0 & 1-\nu/2 \end{bmatrix}, \\
\boldsymbol{D}_s &= \kappa \mu \zeta \boldsymbol{I}_2, \quad \kappa \sim 5/6.
\end{aligned} \tag{4.15b}
$$

As the curvature only involves the normal rotations, we consider the decomposition of deflection, which is devised to avoid shear locking. A portion of the deflection, denoted by w^k, is proposed to construct equivalent Kirchhoff configuration so that

the curvature is the same as what is defined in K-L theory:

$$\begin{aligned}\kappa_x &= -w^k_{,x^2} = -\beta_{x,x},\\ \kappa_y &= -w^k_{,y^2} = -\beta_{y,y},\\ \kappa_{xy} &= -2w^k_{,xy} = -(\beta_{x,y} + \beta_{y,x}).\end{aligned} \tag{4.16}$$

The fact that $\beta_{\alpha,\beta}$ are constants in the C^0 triangular element with linear interpolation suggests a quadratic form for w^k:

$$\begin{aligned}w^k = -((x^2 - x_2x - x_3(x_3 - x_2)y/y_3)\kappa_x\\ + (y^2 - y_3y)\kappa_y + (xy - x_3y)\kappa_{xy})/2 - \alpha_x x - \alpha_y y + \delta.\end{aligned} \tag{4.17}$$

The nodal values in vector form are

$$\left(\boldsymbol{w}^k_J\right) = \begin{bmatrix}1 & 0 & 0\\ 1 & -x_2 & 0\\ 1 & -x_3 & -y_3\end{bmatrix}\begin{bmatrix}\delta\\ \alpha_x\\ \alpha_y\end{bmatrix}. \tag{4.18}$$

In fact δ represents a rigid body translation and is omitted in the following discussion.

Kirchhoff condition is enforced at the three nodes for rotations associated with w^k, for $J = 1, 2, 3$:

$$\begin{aligned}\left(\gamma^k_{xz}\right)_J &= \left(w^k_{,x} - \beta^k_x\right)_J = 0,\\ \left(\gamma^k_{yz}\right)_J &= \left(w^k_{,y} - \beta^k_y\right)_J = 0.\end{aligned} \tag{4.19}$$

From (4.16) and (4.17), we obtain the nodal values of $\boldsymbol{\beta}^k_\alpha$:

$$\begin{aligned}\left[\left(\beta^k_x\right)_J\right] &= \frac{1}{2}\begin{bmatrix}x_2 & 0 & 0\\ -x_2 & 0 & 0\\ -2x_3 + x_2 & 0 & -y_3\end{bmatrix}\begin{bmatrix}\kappa_x\\ \kappa_y\\ \kappa_{xy}\end{bmatrix} - \alpha_x\begin{bmatrix}1\\ 1\\ 1\end{bmatrix},\\ \left[\left(\beta^k_y\right)_J\right] &= \frac{1}{2}\begin{bmatrix}x_3(x_3 - x_2)/y_3 & y_3 & x_3\\ x_3(x_3 - x_2)/y_3 & y_3 & x_3 - x_2\\ x_3(x_3 - x_2)/y_3 & -y_3 & 0\end{bmatrix}\begin{bmatrix}\kappa_x\\ \kappa_y\\ \kappa_{xy}\end{bmatrix} - \alpha_y\begin{bmatrix}1\\ 1\\ 1\end{bmatrix}.\end{aligned} \tag{4.20}$$

Rewriting in the matrix form, we have

$$\boldsymbol{\beta}^k = \boldsymbol{S}\boldsymbol{\kappa} + \boldsymbol{R}^T\boldsymbol{\alpha}. \tag{4.21}$$

Here, $\boldsymbol{S}$ is the matrix of coefficients in (4.20). Other notations are defined by

$$\begin{aligned}
\boldsymbol{\alpha}^{\mathrm{T}} &= [\,\alpha_x \quad \alpha_y\,], \\
\boldsymbol{R} &= \begin{bmatrix} 1 & 0 & 1 & 0 & 1 & 0 \\ 0 & 1 & 0 & 1 & 0 & 1 \end{bmatrix}, \\
\boldsymbol{\kappa}^{T} &= [\,\kappa_x \quad \kappa_y \quad \kappa_{xy}\,], \\
[\boldsymbol{\beta}^k]^T &= \begin{bmatrix} \beta^k_{x1} & \beta^k_{y1} & \beta^k_{x2} & \beta^k_{y2} & \beta^k_{x3} & \beta^k_{y3} \end{bmatrix}.
\end{aligned} \tag{4.22}$$

Recall (4.15), using interpolation and (4.14), we have

$$\begin{aligned}
\boldsymbol{\kappa} &= \boldsymbol{B}^b_r \boldsymbol{\beta}, \\
\boldsymbol{\beta}^k &= \boldsymbol{A}\boldsymbol{\beta} + \boldsymbol{R}^T\boldsymbol{\alpha}, \quad \boldsymbol{A} = \boldsymbol{S}\boldsymbol{B}^b_r.
\end{aligned} \tag{4.23}$$

Assuming no decomposition for $\boldsymbol{\beta}$, we let $\boldsymbol{\beta}^k = \boldsymbol{\beta}$. Solve (4.23) by a left multiplication with $\boldsymbol{R}$

$$\boldsymbol{\alpha} = \boldsymbol{R}(\boldsymbol{I}_6 - \boldsymbol{A})\boldsymbol{\beta}/3. \tag{4.24}$$

Here, we use the relation $\boldsymbol{R}\boldsymbol{R}^T = 3\boldsymbol{I}_2$. The decomposition is then completed with removing the rigid body mode δ:

$$\begin{aligned}
\left(\boldsymbol{w}^k_J\right) = \boldsymbol{w}^k &= -\begin{bmatrix} 0 & 0 & 0 \\ 0 & -x_2 & 0 \\ 0 & -x_3 & -y_3 \end{bmatrix} \begin{bmatrix} \delta \\ \alpha_x \\ \alpha_y \end{bmatrix} = \boldsymbol{X}(\boldsymbol{I}_6 - \boldsymbol{A})\boldsymbol{\beta}/3, \\
\boldsymbol{X} &= \begin{bmatrix} 0 & 0 & 0 & 0 & 0 & 0 \\ x_2 & 0 & x_2 & 0 & x_2 & 0 \\ x_3 & y_3 & x_3 & y_3 & x_3 & y_3 \end{bmatrix}, \\
\boldsymbol{w}^s &= \boldsymbol{w} - \boldsymbol{w}^k, \\
\boldsymbol{\beta}^b &= \boldsymbol{\beta}, \quad \boldsymbol{\beta}^s = 0.
\end{aligned} \tag{4.25}$$

According to (4.15), rotations are wholly responsible for the bending strain energy, whereas w^s alone is responsible for the shear strain energy:

$$2U = \int_A \left(\boldsymbol{\beta}^T(\boldsymbol{B}^b)^T\boldsymbol{D}_b\boldsymbol{B}^b\boldsymbol{\beta} + (\boldsymbol{w}^s)^T(\boldsymbol{B}^s)^T\boldsymbol{D}_s\boldsymbol{B}^s\boldsymbol{w}\right)\mathrm{d}A. \tag{4.26}$$

The implementation for linear application is ready. We may use the power (work rate) to replace the strain energy with incremental formulation when extended to nonlinear problems.

4.2.2 A C^0 Element with Decomposition of Rotations

Alternatively, Kennedy et al. (1986) proposed the decomposition for the rotations:

$$\beta_\alpha = \beta_\alpha^b + \beta_\alpha^s. \tag{4.27}$$

Consider the element configuration to be the same as described in Section 4.2.1. Let $\boldsymbol{\beta}^b$ play the role of Kirchhoff structure with

$$\begin{aligned} w_{,x} - \beta_x^b &= 0, \\ w_{,y} - \beta_y^b &= 0. \end{aligned} \tag{4.28}$$

Note that the quoted paper used different definition for the normal rotations. Here β_x and β_y correspond to $-\theta_y$ and θ_x in the reference paper, respectively. Using the operator matrix described in (4.14) with linear interpolation for deflection, $\boldsymbol{\beta}^b = \boldsymbol{B}_d^s w$, we have

$$\begin{aligned} \beta_x^b &= \frac{y_3(w_2 - w_1)}{x_2 y_3} = \frac{w_2 - w_1}{x_2}, \\ \beta_y^b &= \frac{(x_3 - x_2)w_1 - x_3 w_2 + x_2 w_3}{x_2 y_3} = \frac{(w_3 - w_1)x_2 - (w_2 - w_1)x_3}{x_2 y_3}. \end{aligned} \tag{4.29}$$

These are constants and considered properties of the C^0 triangular element. These relations hold true for the corresponding velocity terms. The physical meaning is implied in a rigid body rotation mode (out of plane). In fact, the constant rotation at all nodes matches rigid body rotation with the same rotating motion. Hence, the rest contents of the normal rotations $\boldsymbol{\beta}^s = \boldsymbol{\beta} - \boldsymbol{\beta}^b$ represent the deformation.

As usual, using $\boldsymbol{B}_r^b$ of (4.14), the rates of membrane strain are

$$\begin{bmatrix} d_x \\ d_y \\ 2d_{xy} \end{bmatrix} = \begin{bmatrix} v_{x,x} \\ v_{y,y} \\ v_{x,y} + v_{x,y} \end{bmatrix}$$

$$= \frac{1}{x_2 y_3} \begin{bmatrix} -y_3 & 0 & y_3 & 0 & 0 & 0 \\ 0 & x_3 - x_2 & 0 & -x_3 & 0 & x_2 \\ x_3 - x_2 & -y_3 & -x_3 & y_3 & x_2 & 0 \end{bmatrix} \begin{bmatrix} V_{x1} \\ V_{y1} \\ V_{x2} \\ V_{y2} \\ V_{x3} \\ V_{y3} \end{bmatrix}. \tag{4.30a}$$

The rates of curvature are calculated from $\dot{\beta}^s$, which is the deformation part of the normal rotation:

$$\begin{bmatrix} \dot{\kappa}_x \\ \dot{\kappa}_y \\ 2\dot{\kappa}_{xy} \end{bmatrix} = \begin{bmatrix} \dot{\beta}^s_{x,x} \\ \dot{\beta}^s_{y,y} \\ \dot{\beta}^s_{x,y} + \dot{\beta}^s_{y,x} \end{bmatrix}$$

$$= \frac{1}{x_2 y_3} \begin{bmatrix} -y_3 & 0 & y_3 & 0 & 0 & 0 \\ 0 & x_3 - x_2 & 0 & -x_3 & 0 & x_2 \\ x_3 - x_2 & -y_3 & -x_3 & y_3 & x_2 & 0 \end{bmatrix} \begin{bmatrix} \dot{\beta}^s_{x1} \\ \dot{\beta}^s_{y1} \\ \dot{\beta}^s_{x2} \\ \dot{\beta}^s_{y2} \\ \dot{\beta}^s_{x3} \\ \dot{\beta}^s_{y3} \end{bmatrix}. \quad (4.30b)$$

The rates of transverse shear strain were suggested in the reference paper:

$$\begin{bmatrix} 2d_{xz} \\ 2d_{yz} \end{bmatrix} = \begin{bmatrix} -\dot{\beta}^s_x \\ -\dot{\beta}^s_y \end{bmatrix} = \boldsymbol{B}^s_\beta \dot{\boldsymbol{\beta}}^s,$$

$$\boldsymbol{B}^s_\beta = \frac{1}{6x_2 y_3} \times \begin{bmatrix} -y_3(2x_2 + x_3) & -(y_3)^2 & y_3(x_3 - 3x_2) & (y_3)^2 & -x_2 y_3 & 0 \\ (x_3)^2 - (x_2)^2 & y_3(x_3 - 2x_2) & x_3(2x_2 - x_3) & -y_3(x_2 + x_3) & x_2(x_2 - 2x_3) & -3x_2 y_3 \end{bmatrix}. \quad (4.30c)$$

The rest of the element formulation and software implementation is straightforward.

4.3 DISCRETE KIRCHHOFF TRIANGULAR ELEMENT

Apart from improving the C^0 element, another method is using the discrete Kirchhoff theory whose early development dates back to the late 1960s, cf. Wempner et al. (1968), Stricklin et al. (1969), and Dhatt (1969, 1970). The element had been "forgotten" for about 10 years, but regained substantial development after being reported by Batoz et al. (1980) as still the most efficient and reliable one among the 9-dof triangular plate bending elements. The nonlinear applications of the Discrete Kirchhoff Triangular (DKT) element can be found in, for example, Bathe et al. (1983) and Wenzel and Schoop (2004). The discrete Kirchhoff theory has also been extended to quadrilateral shell element and axisymmetric shell element. Li et al. (2001), and Wu et al. (2005) reported the application of DKT element, which is implemented in

explicit software for application in the nonlinear transient dynamics. In fact, it is the combination of the DKT plate bending element and a constant strain two-directional (2D) element for membrane stress.

The main idea is using different interpolations for variables and enforcing the element with Kirchhoff conditions at discrete locations to handle the shear locking issue.

The usual three-node linear interpolation is employed for the in-plane motion u_x and u_y, with $2 \times 3 = 6$ unknowns:

$$\begin{aligned} \varphi_1 &= 1 - \xi - \eta, \\ \varphi_2 &= \xi, \\ \varphi_3 &= \eta. \end{aligned} \tag{4.31}$$

The quadratic interpolation with additional three mid-side nodes is used for the normal rotations β_x and β_y, $2 \times 6 = 12$ unknowns:

$$\begin{aligned} \beta_x &= \sum_{J=1}^{6} \beta_{xJ} \quad \psi_J(\xi, \eta), \\ \beta_y &= \sum_{J=1}^{6} \beta_{yJ} \quad \psi_J(\xi, \eta). \end{aligned} \tag{4.32}$$

In the master (parametric) element, shown in Figure 4.3, the shape functions are

$$\begin{aligned} \psi_1 &= (1 - \xi - \eta)(1 - 2\xi - 2\eta), \\ \psi_2 &= \xi(2\xi - 1), \\ \psi_3 &= \eta(2\eta - 1), \\ \psi_4 &= 4\xi\eta, \\ \psi_5 &= 4\eta(1 - \xi - \eta), \\ \psi_6 &= 4\xi(1 - \xi - \eta). \end{aligned} \tag{4.33}$$

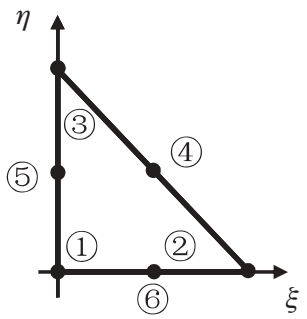

FIGURE 4.3 Triangular element with three mid-points.

For deflection, the element uses two-node Hermite cubic interpolation along each of the three sides. The detailed formula for the element interior is not critical. For example, using parameter s from 0 to 1 along side 1 with node 1 and node 2, we have

$$w|_{\text{Side 1}} = w_1\chi_1 + w_2\chi_2 + w_{1S}\chi_1^1 + w_{2S}\chi_2^1. \tag{4.34}$$

Here, w_{1S} and w_{2S} represent the s-directional derivatives of deflection at the end nodes. The shape functions are

$$\begin{aligned} \chi_1 &= 1 - 3s^2 + 2s^3, \\ \chi_2 &= 3s^2 - 2s^3, \\ \chi_1^1 &= (s - 2s^2 + s^3)L, \\ \chi_2^1 &= (-s^2 + s^3)L. \end{aligned} \tag{4.35}$$

The unknowns introduced are the nodal values and the s-directional derivatives at both ends of each side, total $2 \times 3 + 3 = 9$. So far, a total of 21 unknowns have been introduced for bending and shear.

Now, we impose the discrete Kirchhoff conditions:

(K1) $\gamma_{xz} = \gamma_{yz} = 0$ at the three corner nodes ($2 \times 3 = 6$ constraints).

(K2) The transverse shear strain $\gamma_{zt} = 0$ at three mid-side nodes (3 constraints).

(K3) The rotation component β_n is linear along three sides (3 constraints).

Here, t and n indicate the directions tangential and normal to the sides, shown in Figure 4.4. Note that the rates of β_x and β_y correspond to $-\omega_2$ and ω_1 in Wu et al. (2005), respectively. The rates of β_n and β_t correspond to $-\omega_t$ and ω_n, respectively. Conditions (K1) and (K2) are some remedies to the shear locking corresponding to the case discussed in Section 4.1.3. Condition (K3) is for the C^0-continuity of rotation around element boundaries. In fact, γ_{xz} and γ_{yz} form a 2D vector. Condition (K1) is equivalent to the fact that any component of the shear strain is zero at the corners.

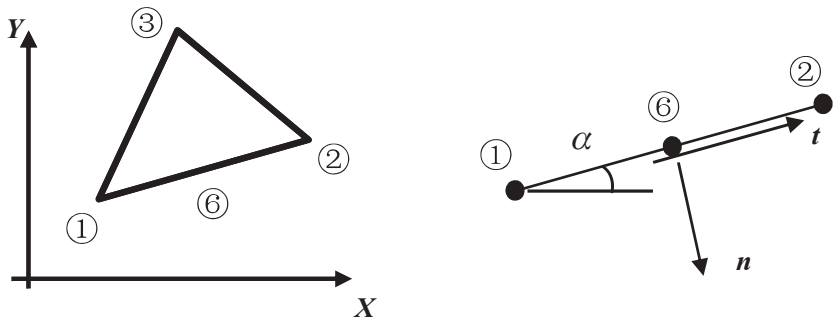

FIGURE 4.4 A side with a mid-point.

Quadratic and cubic interpolations are introduced here for the rotation and deflection, respectively. Other types of discrete Kirchhoff conditions are also possible.

We examine side 3 with nodes 1, 2, and 6 for illustration. Condition (K1) yields

$$\begin{aligned} \gamma_{zt}\Big|_{s=0} &= \left(\frac{\partial w}{L_3 \partial s} - \beta_t\right)\Big|_{s=0} = w_{1S} - \beta_{1t} = 0, \\ \gamma_{zt}|_{s=1} &= w_{2S} - \beta_{2t} = 0. \end{aligned} \tag{4.36}$$

Condition (K2) requires

$$\gamma_{zt}|_{s=0.5} = \frac{3}{2}\frac{w_2 - w_1}{L_3} - \frac{1}{4}(w_{1S} + w_{2S}) - \beta_{6t} = 0. \tag{4.37}$$

Condition (K3) requires

$$\beta_{6n} = (\beta_{1n} + \beta_{2n})/2. \tag{4.38}$$

Express the rotation in a format of 2D vector with (4.36)–(4.38)

$$\begin{aligned} \boldsymbol{\beta}_6 &= \beta_{6t}\boldsymbol{e}_n - \beta_{6n}\boldsymbol{e}_t = \beta_{6y}\boldsymbol{e}_x - \beta_{6x}\boldsymbol{e}_y \\ &= \frac{\boldsymbol{\beta}_1 + \boldsymbol{\beta}_2}{2} + \left(\frac{3}{2}\frac{w_2 - w_1}{L_3} - \frac{3}{4}(\beta_{1t} + \beta_{2t})\right)\boldsymbol{e}_n. \end{aligned} \tag{4.39}$$

With $\boldsymbol{e}_x = \boldsymbol{e}_t \cos\alpha_3 + \boldsymbol{e}_n \sin\alpha_3$ and $\boldsymbol{e}_y = \boldsymbol{e}_t \sin\alpha_3 - \boldsymbol{e}_n \cos\alpha_3$, for $\alpha = 1, 2$, we have $\beta_{\alpha t} = \beta_{\alpha x}\cos\alpha_3 + \beta_{\alpha y}\sin\alpha_3$. With $\boldsymbol{e}_n = \boldsymbol{e}_x \sin\alpha_3 - \boldsymbol{e}_y \cos\alpha_3$, we find

$$\begin{aligned} \beta_{6x} &= 0.5(\beta_{1x} + \beta_{2x}) + (1.5(w_2 - w_1)\cos\alpha_3/L_3 - 0.75((\beta_{1x} + \beta_{2x})\cos\alpha_3 \\ &\quad + (\beta_{1y} + \beta_{2y})\sin\alpha_3))\cos\alpha_3, \\ \beta_{6y} &= 0.5(\beta_{1y} + \beta_{2y}) + (1.5(w_2 - w_1)\sin\alpha_3/L_3 - 0.75((\beta_{1x} + \beta_{2x})\cos\alpha_3 \\ &\quad + (\beta_{1y} + \beta_{2y})\sin\alpha_3))\sin\alpha_3. \end{aligned} \tag{4.40}$$

$\boldsymbol{\beta}_4$ and $\boldsymbol{\beta}_5$ can be obtained by permutation. Thus the derivatives of deflection at corner nodes and the rotation at the mid-side nodes can all be eliminated internally. The system is condensed to three degrees of freedom per node (β_x, β_y, w) for bending-shear, denoted by

$$[\theta_k] = \left(\beta_x^1, \beta_x^2, \beta_x^3, \beta_y^1, \beta_y^2, \beta_y^3, w^1, w^2, w^3\right). \tag{4.41}$$

Utilize the fact that $\psi_1 + (\psi_5 + \psi_6)/2 = \varphi_1$, etc., denote

$$[\Phi_J] = (\varphi_1, \varphi_2, \varphi_3, \psi_4, \psi_5, \psi_6). \tag{4.42}$$

We then obtain the condensed form:

$$\begin{aligned}\beta_x &= \sum_{J=1}^{6} \beta_x^J \psi_J = \sum_{K=1}^{9} \sum_{J=1}^{6} \theta_k (H_x)_{KJ} \Phi_J, \\ \beta_y &= \sum_{J=1}^{6} \beta_y^J \psi_J = \sum_{K=1}^{9} \sum_{J=1}^{6} \theta_k (H_y)_{KJ} \Phi_J.\end{aligned} \tag{4.43}$$

The transformation matrices are derived:

$$(H_x)_{9\times 6} = \begin{bmatrix} \boldsymbol{I}_3 & \begin{bmatrix} 0 & CC_2 & CC_3 \\ CC_1 & 0 & CC_3 \\ CC_1 & CC_2 & 0 \end{bmatrix} \\ \boldsymbol{O}_3 & \begin{bmatrix} 0 & SC_2 & SC_3 \\ SC_1 & 0 & SC_3 \\ SC_1 & SC_2 & 0 \end{bmatrix} \\ \boldsymbol{O}_3 & \begin{bmatrix} 0 & CL_2 & -CL_3 \\ -CL_1 & 0 & CL_3 \\ CL_1 & -CL_2 & 0 \end{bmatrix} \end{bmatrix}, \tag{4.44a}$$

$$(H_y)_{9\times 6} = \begin{bmatrix} \boldsymbol{O}_3 & \begin{bmatrix} 0 & SC_2 & SC_3 \\ SC_1 & 0 & SC_3 \\ SC_1 & SC_2 & 0 \end{bmatrix} \\ \boldsymbol{I}_3 & \begin{bmatrix} 0 & SS_2 & SS_3 \\ SS_1 & 0 & SS_3 \\ SS_1 & SS_2 & 0 \end{bmatrix} \\ \boldsymbol{O}_3 & \begin{bmatrix} 0 & SL_2 & -SL_3 \\ -SL_1 & 0 & SL_3 \\ SL_1 & -SL_2 & 0 \end{bmatrix} \end{bmatrix}. \tag{4.44b}$$

The following notations are used in (4.44): $SL_j = 1.5 \sin\alpha_j / L_j$, $CL_j = 1.5 \cos\alpha_j / L_j$, $SS_j = -0.75 \sin^2\alpha_j$, $CC_j = -0.75 \cos^2\alpha_j$, and $SC_j = -0.75 \sin\alpha_j \cos\alpha_j$.

The rest of the element formulation is rather straightforward. Generally, three-point in-plane quadrature is needed due to inclusion of quadratic shape functions. The application of a two-point quadrature was reported in Li et al. (2001), which provided close results.

It is worth noting that DKT element has more complex formulation than C^0 elements has, which is discussed in previous sections. On the other hand, higher order interpolation used in DKT element requires smaller stable time step. Therefore, it generally uses more computing time than C^0 element does.

4.4 ASSESSMENT OF THREE-NODE R-M PLATE ELEMENT

4.4.1 Evaluations with Warped Mesh and Reduced Thickness

To study the performance of triangular elements, we use the same examples discussed in Section 3.8.1 for quadrilateral elements. We examine C^0 element discussed in Section 4.2.2 and DKT element discussed in Section 4.3. We use the commercial software LS-DYNA V971 to perform the study.

Example 4.1 Twisted beam The problem and parameters were defined by MacNeal and Harder (1985) as one of the test problems, cf. discussion in Example 3.1. A set of four triangular meshes is generated by one-to-two splitting of the quadrilateral meshes, depicted in Figure 4.5. The mesh is graded with a consistent orientation for the triangulation. In this way the triangular mesh has the same number of nodes and double number of elements of the corresponding quadrilateral mesh.

The time history of the displacement at the end point for the original thickness is shown in Figure 4.6. Obviously, the result of C^0 element, shown in Figure 4.6a, is questionable with a tendency to diverge. The maximum displacement at the end point calculated from a fine mesh is away from the reference value, as well as the solution of B-D element or B-L element, which are presented in Example 3.1. The results of DKT element shown in Figure 4.6b seem to converge with small difference

FIGURE 4.5 A triangular mesh of the twisted beam.

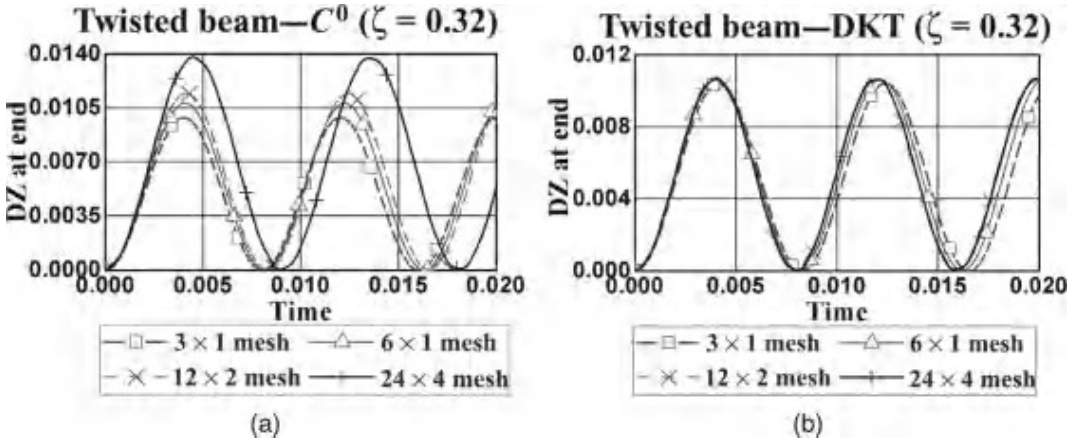

FIGURE 4.6 Solution of the twisted beam problem by the triangular elements: (a) C^0 element; (b) DKT element.

from coarse mesh to fine mesh. The results of DKT element are close to those of B-D element and B-L element. With the reduced thickness 0.032 and 0.0032, load scaling and mass scaling are applied in the same way as discussed in Example 3.1. As shown in Figure 4.7, both results of C^0 element and DKT element converge. The results of C^0 element from the meshes with $40 \times 40 \times 2$ elements and $80 \times 80 \times 2$ elements are close to each other, shown in Figure 4.7a and c, better than what is observed in the case with the original thickness. The results of these two elements are close, and also close to the results of the quadrilateral B-D and B-L elements.

Example 4.2 Hyperbolic paraboloid This example was proposed by Chapelle and Bathe (2003) to study the performance of R-M elements with reduced thickness. It was also used in Wu et al. (2005) to study the performance of DKT element for transient dynamics problem. The problem and parameters are defined in Example 3.2. A set of four triangular meshes is generated by one-to-two splitting of quadrilateral meshes, graded with an alternate orientation to form a cross pattern, and is depicted in Figure 4.8. The triangular mesh has the same number of nodes and double number of elements of the corresponding quadrilateral mesh. Reduction of thickness by 10 times and 100 times with the load scaling and mass scaling is also included in the study.

For thickness equal to 0.1, the results of C^0 element depicted in Figure 4.9 show that convergence has not been achieved with the mesh refinement. But it has a better chance to converge for the case of reduced thickness of 0.01, with fine mesh's result close to DKT's results. The results of DKT element seem to converge, as shown in Figure 4.10. Even with the reduced thickness, the difference in results of DKT element from fine meshes is small. It is also observed that there is a certain type of difference in the results of quadrilateral elements and triangular elements.

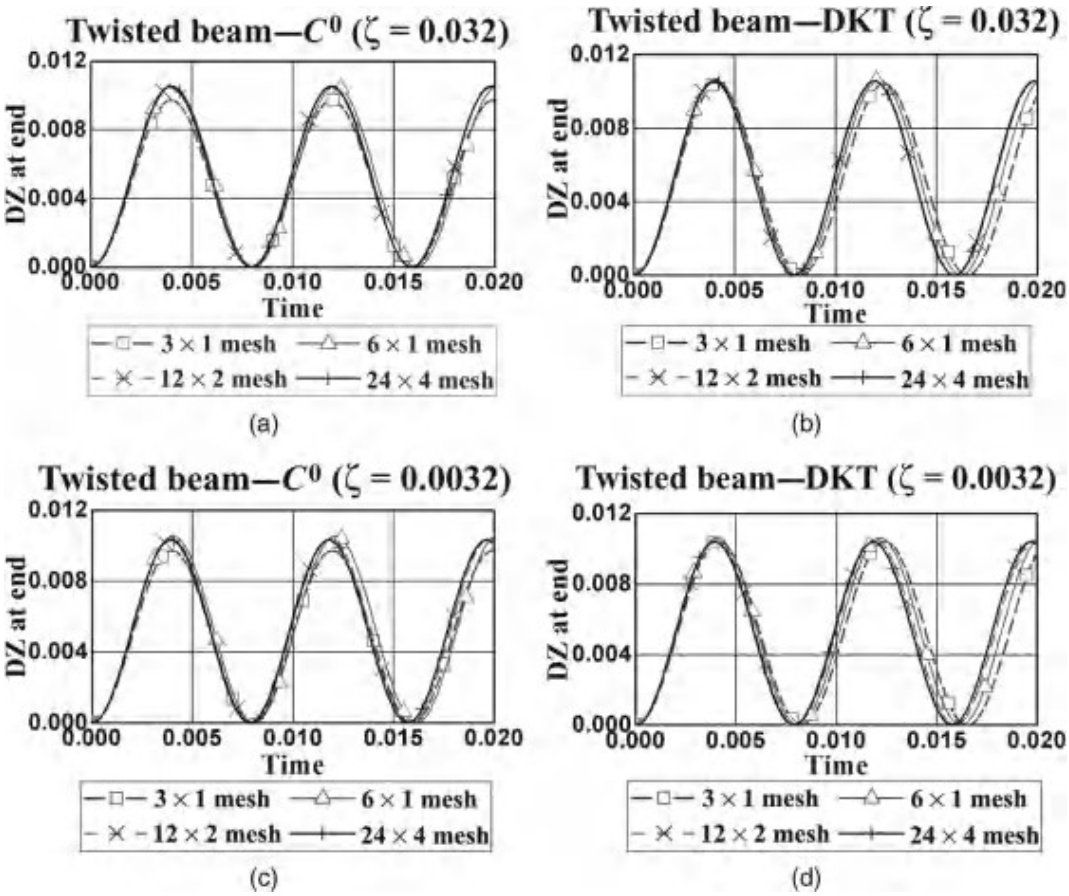

FIGURE 4.7 Solution of the twisted beam problem with reduced thickness by the triangular elements: (a) C^0 element for the reduced thickness 0.032; (b) DKT element for the reduced thickness 0.032; (c) C^0 element for the reduced thickness 0.0032; (d) DKT element for the reduced thickness 0.0032.

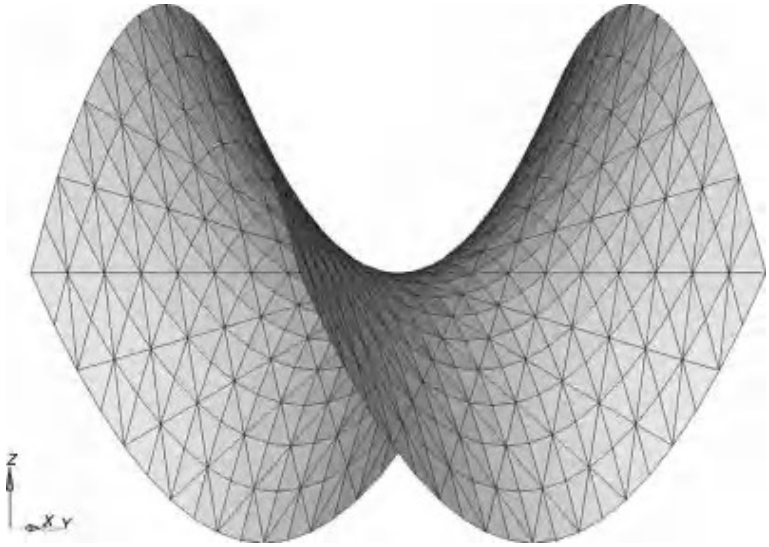

FIGURE 4.8 A triangular mesh of the hyperbolic paraboloid.

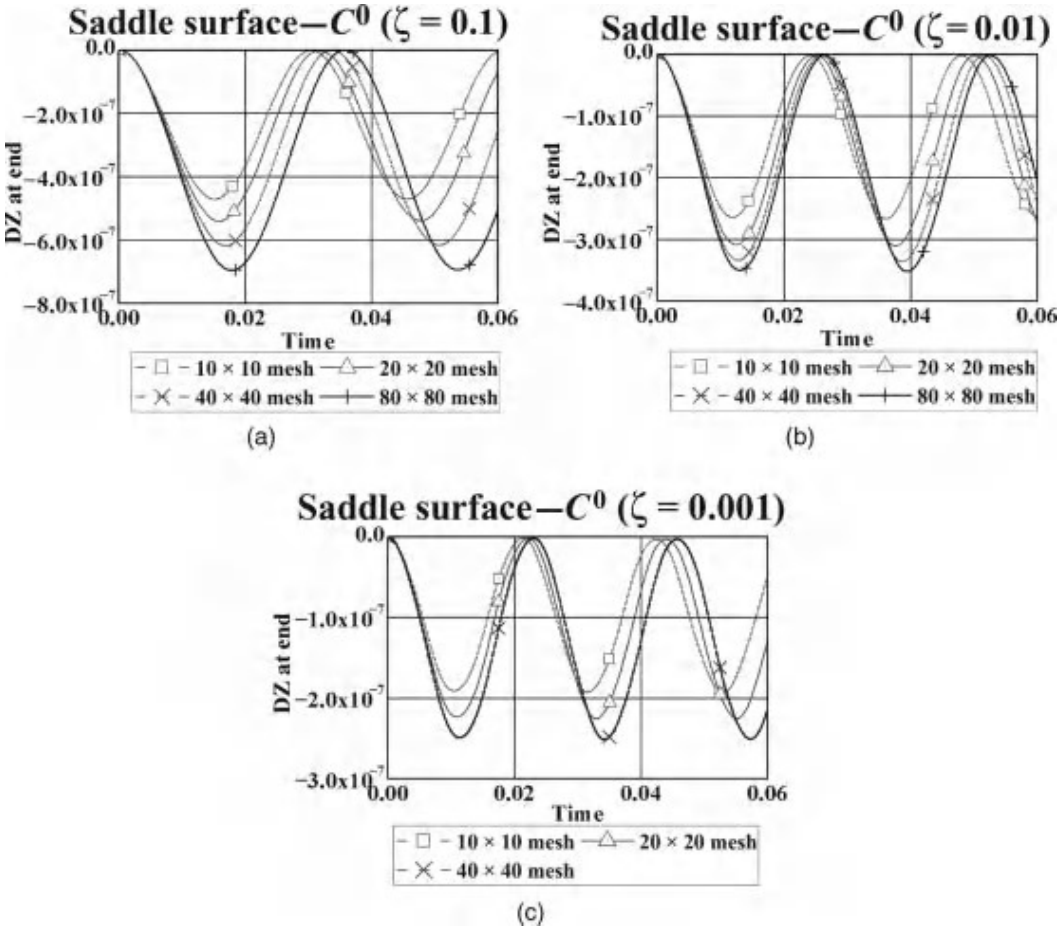

FIGURE 4.9 Solution of the hyperbolic paraboloid problem by the C^0 triangular elements: (a) C^0 element for the original thickness 0.1; (b) C^0 element for the reduced thickness 0.01; (c) C^0 element for the reduced thickness 0.001.

4.4.2 About the Locking-free Low Order Three-node R-M Plate Element

All the developments discussed here have focused on the subject of removing shear locking. Unfortunately, like the quadrilateral elements discussed in Chapter 3, these elements have not been proven to be locking-free even for static linear applications. The first recognized locking-free R-M element was developed by Arnold and Falk (1989). It was a three-node element using nonconforming method. The rotations used linear interpolation plus one cubic bubble function $\lambda_1\lambda_2\lambda_3$ (expressed in barycentric coordinates), which was condensed inside the element. The deflection used nonconforming linear interpolation with element continuity at mid-points of the three sides only. The transverse shear strains were approximated by piecewise constants and were discontinuous cross the elements.

Durán and Liberman (1992) developed a locking-free triangular element using low order interpolation with the same concept of the rival four-node element

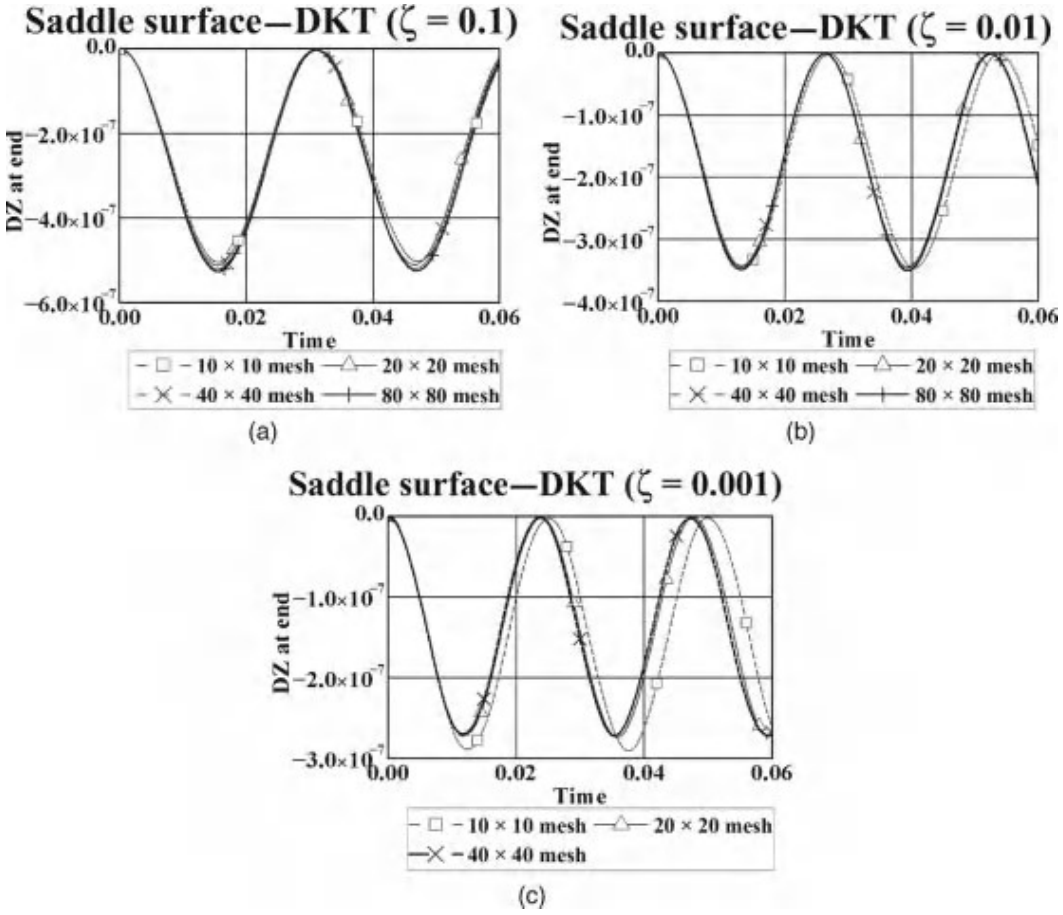

FIGURE 4.10 Solution of the hyperbolic paraboloid problem by the DKT triangular elements: (a) DKT element for the original thickness 0.1; (b) DKT element for the reduced thickness 0.01; (c) DKT element for the reduced thickness 0.001.

described in Section 3.8.2. The rotations used linear interpolation plus the span of edge bubble functions. The transverse shear strains used the rotation of the lowest order Raviart–Thomas space.

Locking-free elements with quadratic or higher order interpolation for rotations or deflection have also been developed; see Falk and Tu (2000) and Arnold et al. (2002) for commentaries. These elements used bubble functions, or nonconforming approaches, etc. Their development has never been a simple task. The implementation of these elements for general applications of nonlinear transient dynamic problems deserves further investigations.